International Journal of Recent Development in Engineering and Technology
Website: www.ijrdet.com (ISSN 2347-6435 (Online) Volume 15, Issue 08, August 2026)

A Deep Feature Fusion Framework for Cerebral Aneurysm Detection Using DenseNet and Vision Transformer

Tamilarasi. S[1], Dr. Shanthi Sona[2]
[1]*Research Scholar, Computer Science, Tiruppur Kumaran College for Women, India*
[2]*Research Supervisor, Assistant Professor, PG & Research Department of Computer Science, Tiruppur Kumaran College for Women, India*

Abstract-- **Cerebral aneurysm is a potentially life-threatening cerebrovascular abnormality characterized by a localized dilation or bulging of an arterial wall. Early identification of an aneurysm is important because rupture can result in subarachnoid hemorrhage and severe neurological complications. Computed Tomography Angiography (CTA) is widely used for non-invasive visualization of cerebral blood vessels; however, the identification of small aneurysms in CTA images remains challenging because of complex vascular structures, low contrast, anatomical variations, classification, and similarities between aneurysms and normal vessel bifurcations. Recent developments in deep learning have demonstrated considerable potential for assisting radiologists in aneurysm detection. Nevertheless, conventional convolutional neural networks may have difficulty representing long-range spatial relationships, whereas transformer-based models generally require substantial computational resources and large training datasets.**

Keywords-- **Cerebral aneurysm, CT angiography, deep learning, DenseNet, Vision Transformer, shifted-window transformer, attention mechanism, medical image analysis, aneurysm detection.**

I. INTRODUCTION

Cerebral aneurysms are abnormal focal dilatations of intracranial arteries and represent an important clinical concern because rupture may lead to subarachnoid hemorrhage, permanent neurological disability, or death. The diagnosis and management of intracranial aneurysms depend on several factors, including aneurysm size, location, morphology, patient characteristics, and rupture status. In clinical practice, imaging plays an important role in identifying aneurysms and evaluating their anatomical characteristics.

Computed Tomography Angiography (CTA) has become an important non-invasive imaging modality for the evaluation of cerebral vasculature. CTA provides detailed information about the lumen and morphology of cerebral blood vessels and can be acquired relatively quickly.

However, interpretation of CTA examinations can be difficult when aneurysms are small, located near complex vascular structures, or associated with calcifications and other anatomical variations. In addition, the large volume of image data generated during a CTA examination can increase the workload of radiologists.

II. RELATED WORKS

The exact shape of intracranial aneurysms is pivotal in diagnosing medial images and surgical planning. While voxel-based DL algorithms have been presented for this segmentation, their performance remains constrained. A two-step surface-based DL pipeline achieving notably better results with improved accuracy was presented in [6]. A method to reduce false positive employing convolutional neural network transformer was proposed in [7] via segmentation mask. However in case of robust in diverse clinical settings the accuracy factor was not facilitated. To address on this research gap an IA visualization enhancement technique improving clinical workflow efficient was presented in [8]. A systematic review of AI in aneurysm detection was investigated in [9]. However there exist drawbacks in incorporating CTA with clinical scores (PHASES) to predict IAs rupture risk. A meta-analysis measuring AI algorithm performance for predicting IAs rupture risk based on CTA was investigated in [10].

III. MATERIALS AND METHODOLOGY

Intracranial aneurysms (IA) are becoming gradually frequent with advancement observed in imaging technology. With regard to the aneurysms detection from several imaging modalities, the likelihood of being not noticed occurs chiefly owing to the minuscule size and complicated structure. Artificial intelligence (AI), with its unprecedented potentialities in image-based tasks has put away scholarly interest globally. The application of AI in the operation of IAs being encouraging for promoting medical research and patient care.

International Journal of Recent Development in Engineering and Technology
Website: www.ijrdet.com (ISSN 2347-6435 (Online) Volume 15, Issue 08, August 2026)

Employing deep learning techniques, AI evinces exceptional potentialities in precisely obtaining and segmenting aneurysms, notably improving diagnostic sensitivity and accuracy. In this work an artificial intelligence (AI) to detect aneurysm by applying Ternary View DenseNet and Shifted Window Vision Transformer (TVDN-SWViT) is designed. Figure 1 shows the architecture of TVDN-SWViT method.

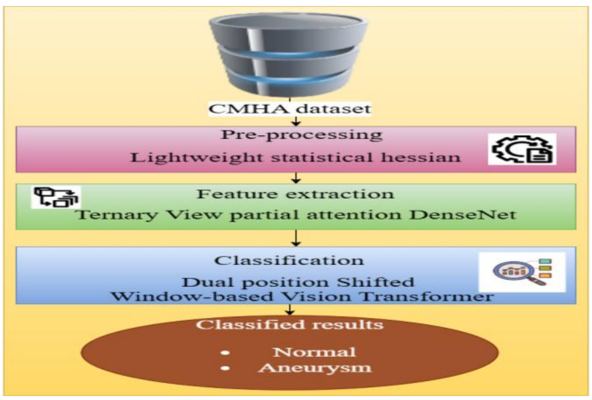

Figure 1 Architecture of TVDN-SWViT method

As illustrated in the above figure 1, first intracranial aneurysm image were accumulated and thereafter experienced brain skull stripping and vessel enhancement processes as part of the preprocessing stage using Lightweight Statistical Hessian.

3.1 Data Preparation and Pre-processing

The CMHA dataset extracted from comprises of comprehensive medical imaging data obtained from 99 patients and 44 healthy controls. Each patient's record consist raw CTA images, 3D models and hemodynamic analysis results for both aneurysm detection. The data for healthy controls comprises raw CTA images of healthy arteries. Also patient identifiers were coded uniformly with 'AHMU1218', denoting Anhui Medical University in addition to the data collection period between 2012 and 2018, followed by a three-digit unique patient number.

3.2 Lightweight Statistical Hessian-based Pre-processing

The high resolution CMHA-Intracranial Aneurysm dataset employed in our work is pre-processed with the objective of isolating the brain vasculature with other and therefore reduce the noise. In our work Lightweight Statistical Hessian-based Pre-processing model is applied.By applying these functionalities via multi-scale analysis of Hessian matrix tubular structures in turn improve the contrast-to-noise ratio in the CTA volumes. Figure 2 shows the structure of Lightweight Statistical Hessian-based Pre-processing model.

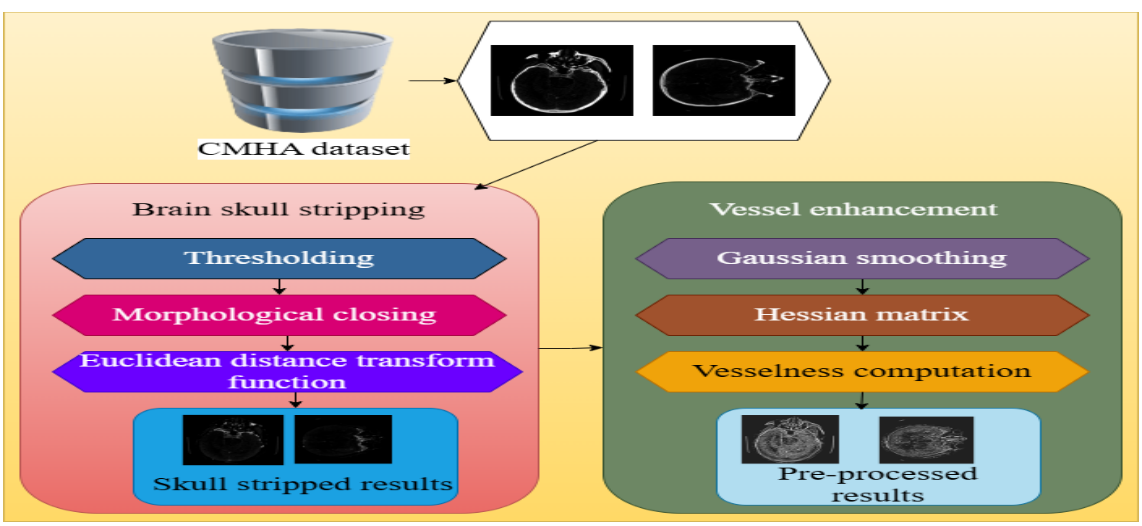

Figure 2 Structure of Lightweight Statistical Hessian-based Pre-processing

International Journal of Recent Development in Engineering and Technology
Website: www.ijrdet.com (ISSN 2347-6435 (Online) Volume 15, Issue 08, August 2026)

The above figure 2 portrait Lightweight Statistical Hessian-based Pre-processing model is split into two processes. They are brain skull stripping and vessel enhancement.

$$Th(p,q)=\begin{cases}255, & if\ Int[S(p,q)]>\delta \\ 0, & if\ Int[S(p,q)]\leq\delta\end{cases} \quad (1)$$

From the above equation (1) 'Int' denotes the intensity of the sample images 'S' located at coordinates 'p,q'. Also a binary mask indicating '255' (i.e. white) for skull and high intensity structures, other pixels of images were assigned '0' (i.e. black).To focus on this aspect, morphological closing operation is carried out utilizing a '20*20' kernel as given below.

$$MCK=[Int(S)]_{20*20} \quad (2)$$

The Euclidean Distance Transform-based Refinement used in our work evaluates the minimum distance from each foreground pixel to the subsequent adjacent nearest background pixel as given below.

$$Res=Dis(p,q)=\min\sqrt{(p-p')^2+(q-q')^2} \quad (3)$$

From the above equation (3) '$Dis(p,q)$' denotes the distance resultant value at pixel 'p,q'. The distance function identifies the subsequent adjacent nearest background pixel '(p,q)' and measures Euclidean distance.

Pixels with minimal '$Dis(p,q)$' resultant values are found to be closer to the background and probably belong to skull.The Hessian matrix of the skull stripped image in the 's' scale at '$Int(Res)$' or 'Res' is defined as given below.

$$H_{Res,s}=\begin{bmatrix}\frac{\partial^2 Int(Res,s)}{\partial Res_1^2} & \frac{\partial^2 Int(Res,s)}{\partial Res_1 Res_2} \\ \frac{\partial^2 Int(Res,s)}{\partial Res_2 Res_1} & \frac{\partial^2 Int(Res,s)}{\partial Res_2^2}\end{bmatrix} \quad (4)$$

From the above matrix results obtained from partial derivatives is found to be sensitive to noise and hence to minimize the effects of image noise, the image intensities are initially convoluted with Gaussian filter as given below.

$$GF(Res,s)=\frac{1}{2\pi s^2}e^{\frac{-|p-q|^2}{2s^2}} \quad (5)$$

From the above equation (5) '$|p-q|^2$' denotes the spatial neighborhood of 'p' along with 's' as scale factor to highlight arteries. Then, the normalized Hessian-based Vessel Enhancement filter is denoted as given below.

$$PS=H_{Res,s}[GF(Res,s)] \quad (6)$$

From the above equation (6) by obtaining resultant pre-processed samples 'PS' aids in efficiently differentiating between blood vessels and neighboring or adjacent tissues.

Algorithm 1 Lightweight Statistical Hessian-based Pre-processing

Input: Dataset 'DS', Sample Images '$S=\{S_1,S_2,\ldots,S_N\}$'
Output: Noise reduced and enhanced pre-processed samples

Initialize 'N=143'
Begin
For each Dataset 'DS' with Sample Images 'S'
Evaluate threshold according to (1) for eliminating high-intensity structures
Evaluate morphological closing operation according to (2) for bridging fragmented brain regions and fill small holes
Evaluate Euclidean Distance Transform-based Refinement according to (3) for strengthening segregation between brain and non-brain structures
Return skull stripped results
Generate vessel enhancement results according to (4) and (5)
Return vessel enhanced results
Return pre-processed sample results
End for
End

As given in the above algorithm with the sample images obtained from the CMHA dataset are subjected to two different processes. They are skull stripping and vessel enhancement.

3.3 Ternary View Partial Attention DenseNet Feature extraction-based Artificial Intelligence model

Feature extraction helps identify small protrusions that are found to be demanding to detect. This is owing to the size of small aneurysms therefore making in difficult to differentiate between normal and aneurysm. Figure 3 shows the structure of Ternary View Partial Attention DenseNet Feature extraction model.

International Journal of Recent Development in Engineering and Technology
Website: www.ijrdet.com (ISSN 2347-6435 (Online) Volume 15, Issue 08, August 2026)

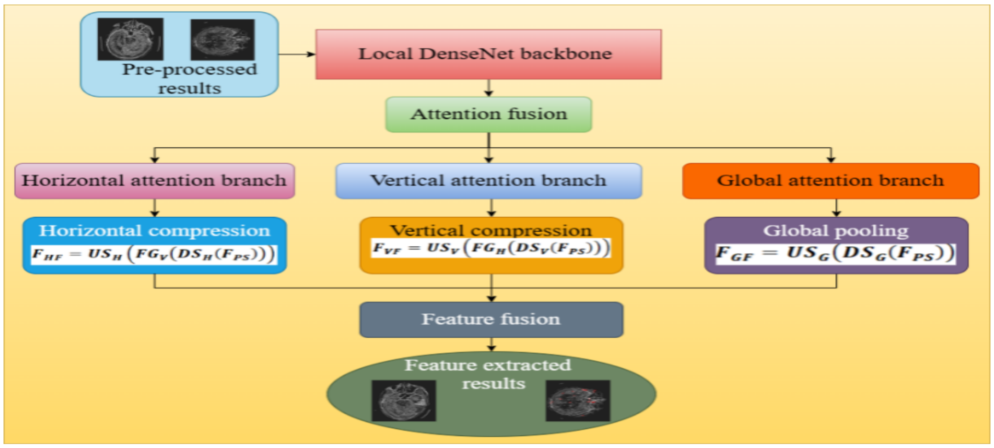

Figure 3 Structure of Ternary View Partial Attention DenseNet Feature extraction model

Figure 3 portrayed, the DenseNet feature extraction employed for aneurysm detection in CT Angiography (CTA) images directly learns to identify vascular abnormalities by reusing features across multiple layers, instead of depending on high-level features.

For horizontal and vertical branches the pre-processed sample input feature '$F_{PS} \in R^{H*W}$' is compressed horizontally '$F_H \in R^{1*W}$' and vertically '$F_V \in R^{H*1}$' respectively. Following which the branch horizontal feature '$F_{HF} \in R^{H*W}$ and vertical feature '$F_{VF} \in R^{H*W}$' is obtained after detail extraction. The horizontal and vertical branch feature results are obtained as given below.

$$F_{VF} = US_V\left(FG_H\left(DS_V(F_{PS})\right)\right) \quad (7)$$

$$F_{HF} = US_H\left(FG_V\left(DS_H(F_{PS})\right)\right) \quad (8)$$

From the above equations (7) and (8) 'DS_H' denote the horizontal and vertical 'DS_V' down sampling of feature maps are performed on the pre-processed sample input feature 'F_{PS}'. On the other hand, using the up-sampling function 'US_V' and 'US_H' integrates high-resolution details from early layers with deeper information to differentiate aneurysm boundaries accurately. Finally, the horizontal 'FG_H' and vertical 'FG_V' results extract both fine-grained low-level and high-level visual structural features. This is mathematically defined as given below.

$$F_{GF} = US_G\left(DS_G(F_{PS})\right) \quad (9)$$

$$FE = F_{PS} \otimes \sigma(F_{VF} \oplus F_{HF} \oplus F_{GF}) \quad (10)$$

From the above equations (9) and (10) the three branch features i.e., horizontal, vertical along with global and pre-processed sample input feature 'F_{PS}' are fused to obtain the output or the feature extracted results 'FE'. The pseudo code representation of Ternary View Partial Attention DenseNet Feature extraction-based Artificial Intelligence is given below.

Algorithm 2 Ternary View Partial Attention DenseNet Feature extraction-based Artificial Intelligence

Input: Dataset '*DS*', Sample Images '$S = \{S_1, S_2, \ldots, S_N\}$'
Output: false positive-minimized feature extraction

Initialize 'N=143', pre-processed sample results '*PS*'
Begin
For each Dataset '*DS*' with Sample Images '*S*' and pre-processed sample results '*PS*'
Generate horizontal branch feature results according to (7)
Generate vertical branch feature results according to (8)
Generate global branch feature results according to (9)
Obtain feature extracted results according to (10)
Return feature extracted results '*FE*'
End for
End

As mentioned in the above algorithm the entire process of Ternary View Partial Attention DenseNet Feature extraction-based Artificial Intelligence is split into three parts.

3.4 Dual Position Shifted Window-based Vision Transformer for Aneurysm Detection

Finally, the proposed method uses a specific kind of image classification model called Dual Position Shifted Window-based Vision Transformer for performing a binary classification on aneurysm CTA medical images. They are Patch Embedding, Dual Position Encoding and Shifted Window Transformer Encoder for Aneurysm Detection. Figure 4 shows the structure of Dual Position Shifted Window-based Vision Transformer for Aneurysm Detection.

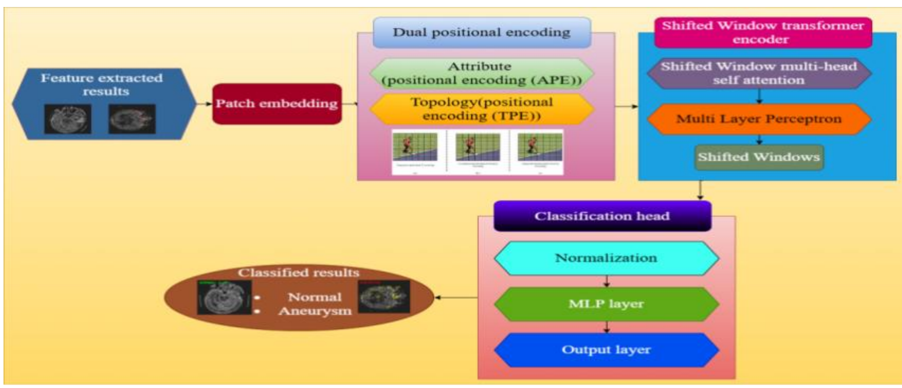

Figure 4 Structure of Dual Position Shifted Window-based Vision Transformer for Aneurysm Detection

Figure 4 portrayed, the extracted features are flattened and converted into a sequence of embeddings or tokens and fed into the Vision Transformer. The proposed classifier method for aneurysm detection initiates the process by splitting the input image (i.e. pre-processed and feature extracted results '$X \in PS[FE]$' into a fixed number of patches. Let us consider an input image '$X \in R^{H*W*C}$' with 'C', 'H' and 'W' denoting the channel number, image height and image width respectively. The first step is patching embedding, where the image is split into 'M' image pieces, where '$M=\frac{H*W}{Size^2}$' with '$Size$' denoting the patch size. Then, these image pieces are flattened as a vector with size of '$Size^2C$' and projected to a lower dimension as given below.

$$Out_i = W.x_i + b \qquad (11)$$

From the above equation (11) 'W' denotes the learnable weight matrix for the corresponding flattened input image 'x_i' and storing their corresponding results 'Out_i' to the image vector after projection. Initially 'l' clusters '$C=\{C_1, C_2, \ldots, C_l\}$' based on the pre-processed and feature extracted results 'X' are formed. Then the centroid representation 'X_i^{Cen}' of a cluster 'C' is evaluated as given below.

$$X_i^{Cen} = \frac{1}{|C_i|} \sum X_j \qquad (12)$$

Based on the above results the APE result 'X^{APE}' of 'X_j' belonging to cluster 'C_i' is defined as given below.

$$X_j^{APE} = Cosine\left(X_j, X_i^{Cen}\right) \qquad (13)$$

From the above equation (13) result ensures that the samples within the same cluster generate more similar positional encoding representations than those in different clusters. In addition, the proposed method incorporated TPE to generate the final dual positional encoding result as given below.

$$Res = X^{DPE} = X^{APE} \| X^{TPE} \qquad (14)$$

From the above equation (14) the dual positional encoder results of the provided samples 'X^{DPE}' are arrived at by concatenating '$\|$' the results of APE 'X^{APE}' and TPE 'X^{TPE}' (i.e. eigen vector matrix corresponding to non-trivial eigen values) respectively.The normalization layer is denoted as given below.

$$Norm(x) = \frac{x-\mu}{\sqrt{\sigma^2+\epsilon}} \qquad (15)$$

From the above equation (15), using 'μ', 'σ' and 'ϵ' denotes the mean, variance of vector and constant serves as a mechanism to standardize data for further processing.

International Journal of Recent Development in Engineering and Technology
Website: www.ijrdet.com (ISSN 2347-6435 (Online) Volume 15, Issue 08, August 2026)

The Shifted Window function employed in our work constrains self-attention calculations to non-overlapping patches, allowing the method to concentrate on the detailed texture and shape of prospective aneurysms without analyzing the entire 3D volume at once, hence minimizing overall training time.

$$Res^{(k+1)}=\left(Norm(x)\left(Res^{k}\right)\right)+\left(Res^{k}\right) \quad (16)$$

$$Res^{(k+2)}=MLP\left(Norm(x)\left(Res^{k+1}\right)\right)+\left(Res^{k+1}\right) \quad (17)$$

$$Q=XW_Q;K=XW_K;V=XW_V \quad (18)$$

Finally the attention formula results are obtained by shifting the window partitioning between layers as given below.

$$Att(Q,K,V)=\left[Res^{(k+1)},Res^{(k+2)},\ldots\right] softmax\left(\frac{QK^T}{\sqrt{d}}\right)V \quad (19)$$

From the above equation (19) finally the classified results are obtained by applying the scaling factor 'd' denoting the dimension of query, key and value vectors respectively.This procedure is repeated iteratively for 'k' layers to generate the final output. The pseudo code representation of Dual Position Shifted Window-based Vision Transformer for Aneurysm Detection is given below.

Algorithm 3 Dual Position Shifted Window-based Vision Transformer for Aneurysm Detection

Input: Dataset 'DS', Sample Images '$S=\{S_1,S_2,\ldots,S_N\}$'
Output: accuracy aneurysm detection

Initialize 'N=143', pre-processed sample results 'PS', feature extracted results 'FE'
Begin
For each Dataset 'DS' with Sample Images 'S', pre-processed sample results 'PS' and feature extracted results 'FE'
Patch Embedding
Flatten the image pieces as a vector according to (11)
Dual Positional Encoding
Evaluate the centroid representation 'X_i^{Cen}' of a cluster 'C' according to (12)
Evaluate the Attribute-based Positional Encoding results according to (13)
Evaluate the dual positional encoding result according to (14)
Return dual positional encoding result
Transformer Encoder
Generate normalization results according to (15)
Evaluate Shifted Window function results according to (16), (17) and (18)
Classification Head
Generate classification head results according to (19)
Return classified output
End for
End

As given in the above algorithm Dual Position Shifted Window-based Vision Transformer for Aneurysm Detection is split into four parts. They are patch embedding, dual position encoding, transformer encoder and classification head.

IV. Case Study And Implications

In this section case analysis of aneurysm detection using CTA images are simulated by applying Ternary View DenseNet and Shifted Window Vision Transformer (TVDN-SWViT). As already stated the aneurysm samples can be sliced into multiple images.

In our work to perform simulation two aneurysm subjects with subject ID AHMU1218052, AHMU1218052 and one healthy CTA image with subject ID AHMU1218104 are used for simulation. For simulation purpose with 546 slides, 561 slides and 863 slides present in three subjects, slice number 385, slice number 415, slice number 416, slice number 417 and slice 446 are used for subject ID AHMU1218052. In a similar manner, slice number 389, slice number 423, slice number 424, slice number 425 and slice number 458 are used for subject ID AHMU1218052.First, Lightweight Statistical Hessian-based Pre-processing is applied to the above set of samples and their results are shown separately for skull stripping and vessel enhanced slice results.

International Journal of Recent Development in Engineering and Technology
Website: www.ijrdet.com (ISSN 2347-6435 (Online) Volume 15, Issue 08, August 2026)

Subject_id	Slices				
AHMU1218052	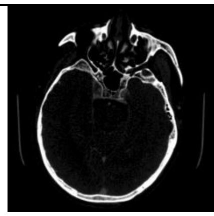 Slice_385	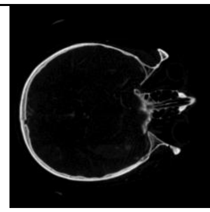 Slice_415	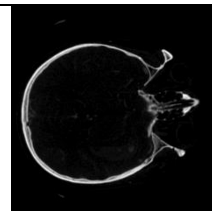 Slice_416	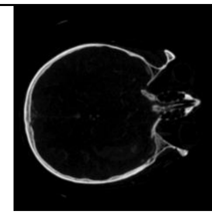 Slice_417	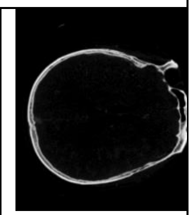 Slice_446
Skull Stripped results	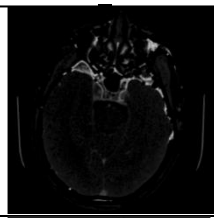	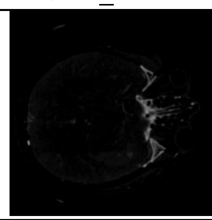	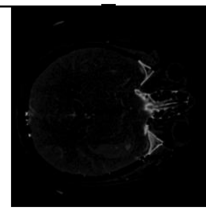	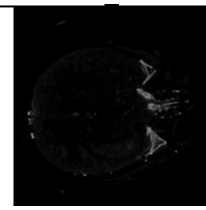	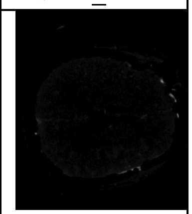
Vessel enhanced results		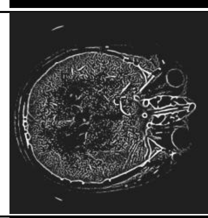	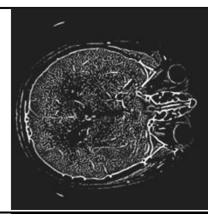	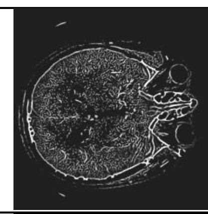	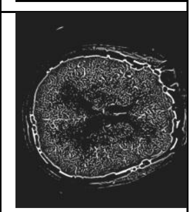
AHMU1218053	 Slice_389	 Slice_423	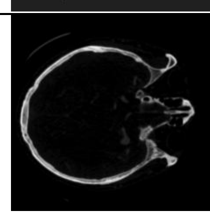 Slice_424	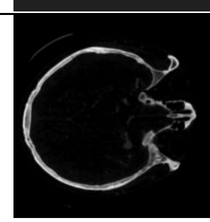 Slice_425	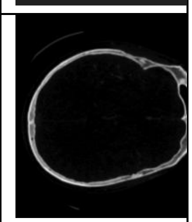 Slice_458
Skull Stripped results	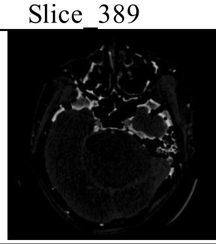	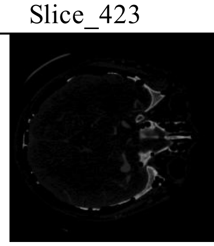	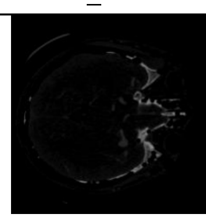	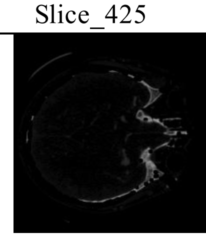	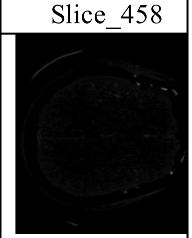
Vessel enhanced results		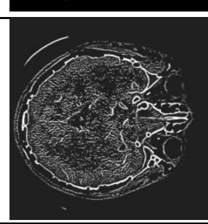	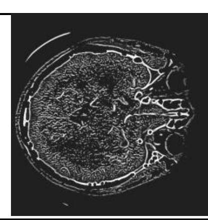	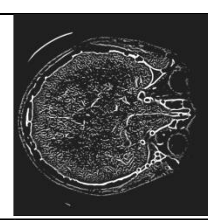	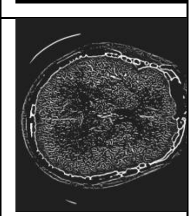
AHMU1218104 (Healthy)	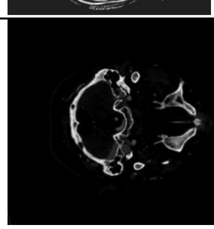 Slice_529	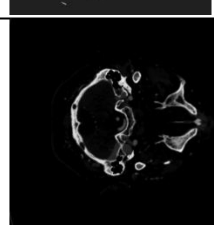 Slice_530	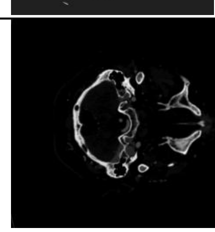 Slice_531	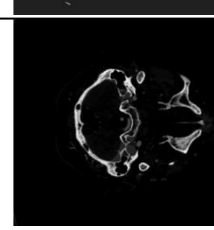 Slice_532	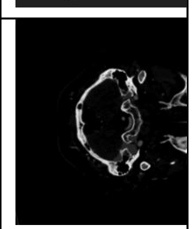 Slice_533

Skull Stripped results	
Vessel enhanced results	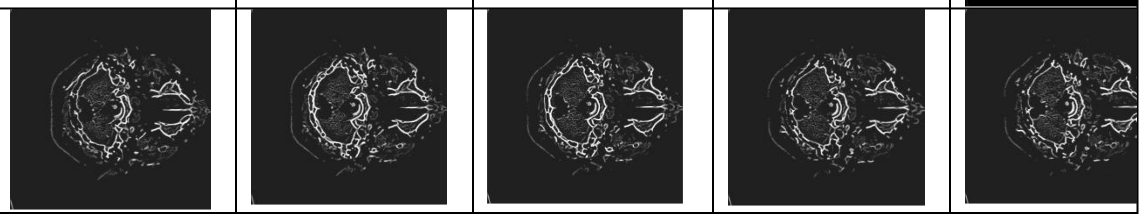

Figure 5 Lightweight Statistical Hessian-based Pre-processing

As given in the above figure 5 the results of pre-processing separately for skull stripping and vessel enhancement are applied. By applying this process improves the noise ratio.

V. Experimental Setup And Discussion

The proposed artificial intelligence (AI) application to screen aneurysm detection using Ternary View DenseNet and Shifted Window Vision Transformer (TVDN-SWViT) is evaluated employing Python working on MS Window platform on computer with i3-2350 processor and 2 GB RAM. The results are compared with the previous two existing methods.PSNR, false positive rate, precision, recall and accuracy using CMHA dataset extracted from Figshare.

5.1 Performance analysis of Peak Signal to Noise Ratio

Peak Signal-to-Noise Ratio (PSNR) is a pivotal performance metric utilized in the detection of aneurysm. Higher PSNR values represent lower noise with better image quality, therefore facilitating enhanced diagnostic accuracy, like increasing aneurysm detection and vice versa.

$$PSNR=10*log_{10}\left(\frac{Max_S^2}{MSE}\right) \qquad (20)$$

$$MSE=\frac{1}{m*n}\sum_{p=1}^{m}\sum_{q=1}^{n}[GT(p,q)-NI(p,q)]^2 \qquad (21)$$

From the above equations (20) and (21) the results of peak signal to noise ratio '*PSNR*' and mean square error '*MSE*' results are arrived at based on the maximum possible pixel value of sample image 'Max_S^2', ground truth image '*GT*', noisy image '*NI*' with respect to '*m*' rows and '*n*' columns respectively. Table 1 given below lists the results of PSNR by substituting the values in equations (20) and (21) using the three methods, TVDN-SWViT, UJ-CPS [1] and CNN-based DLM [2].

Table 1 PSNR results

Image size (KB)	PSNR (dB)		
	TVDN-SWViT	UJ-CPS [1]	CNN-based DLM [2]
26.1	28.25	23.15	21.55
26.5	27.35	22.55	20.35
34.9	25	20.25	18.55
36.3	24.15	19.55	17.35
36.8	23	18.15	16.55
37.4	22.45	17.35	15.25
37.8	21	16.55	14.15
63.8	20.85	15.35	13.25
65.3	19.35	14.25	12.15
65.9	18.15	13.55	11.55

International Journal of Recent Development in Engineering and Technology
Website: www.ijrdet.com (ISSN 2347-6435 (Online) Volume 15, Issue 08, August 2026)

Figure 8 PSNR versus image size

Figure 8 illustrates the graphical representation of PSNR using three methods TVDN-SWViT, UJ-CPS [1] and CNN-based DLM [2]. Ten different subjects with image sizes ranging between 26.1KB and 65.9KB were used to analyze the results of PSNR.

5.2 Performance analysis of False Positive Rate

The false positive rate in the detection of aneurysm denotes cases where CTA imaging incorrectly identifies a normal vascular structure or anatomical variant as an aneurysm. This is mathematically defined as given below.

$$FPR = \frac{FP}{FP+TN} \quad (22)$$

From the above equation (22) the false positive rate '*FPR*' is evaluated based on the false positive rate '*FP*' and true negative rate '*TN*' respectively. Table 2 given below lists the results of PSNR by substituting the values in equation (22) using the three methods, TVDN-SWViT, UJ-CPS [1] and CNN-based DLM [2].

Table 2 False Positive Rate results

Sample (slices)	False Positive Rate		
	TVDN-SWViT	UJ-CPS [1]	CNN-based DLM [2]
500	0.37	0.58	0.72
1000	0.41	0.6	0.74
1500	0.48	0.62	0.76
2000	0.55	0.65	0.78
2500	0.59	0.68	0.79
3000	0.65	0.72	0.8
3500	0.55	0.68	0.75
4000	0.48	0.65	0.72
4500	0.45	0.67	0.7
5000	0.4	0.6	0.68

International Journal of Recent Development in Engineering and Technology
Website: www.ijrdet.com (ISSN 2347-6435 (Online) Volume 15, Issue 08, August 2026)

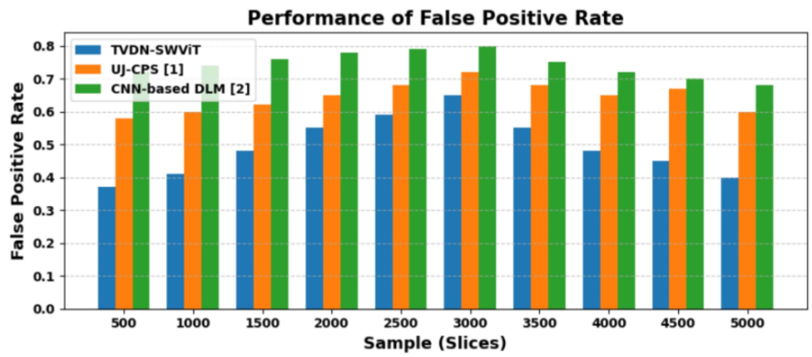

Figure 9 False Positive Rate versus sample slices

Figure 9 illustrates representation of false positive rate using proposed TVDN-SWViT and two existing methods, UJ-CPS [1] and CNN-based DLM [2].

5.3 Performance analysis of Precision, Recall and Accuracy

Precision refers to the potentiality of a classifier method to not label a negative sample as positive. Recall on the other hand defines the potentiality of a classifier method to identify all positive samples.Finally, accuracy refers to the ratio of correctly predicted aneurysm observations to the total observations.

$$Pre=\frac{TP}{TP+FP} \quad (23)$$

$$Rec=\frac{TP}{TP+FN} \quad (24)$$

$$Acc=\frac{TP+TN}{TP+FP+TN+FN} \quad (25)$$

From the above equations (23), (24) and (25) precision '*Pre*', recall '*Rec*' and accuracy '*Acc*' is evaluated based on the true positive rate '*TP*' (i.e. normal samples detected as normal), false positive rate '*FP*' (i.e. normal samples detected as aneurysm), true negative rate '*TN*' (i.e. aneurysm samples detected as aneurysm) and false negative rate '*FN*' (i.e. aneurysm samples detected as normal). Table 3 given below lists the results of Precision, Recall and Accuracy by substituting the values in equations (23), (24) and (25) using TVDN-SWViT, UJ-CPS [1] and CNN-based DLM [2].

Table 3 Precision, Recall and Accuracy results

Samples	Precision			Recall			Accuracy		
	TVDN-SWViT	UJ-CPS [1]	CNN-based DLM [2]	TVDN-SWViT	UJ-CPS [1]	CNN-based DLM [2]	TVDN-SWViT	UJ-CPS [1]	CNN-based DLM [2]
500	0.96	0.94	0.91	0.98	0.97	0.96	0.96	0.92	0.89
1000	0.94	0.81	0.76	0.95	0.83	0.77	0.93	0.85	0.75
1500	0.92	0.79	0.74	0.93	0.81	0.75	0.91	0.83	0.73
2000	0.9	0.74	0.69	0.91	0.79	0.73	0.88	0.8	0.7
2500	0.88	0.75	0.7	0.84	0.72	0.66	0.85	0.77	0.67
3000	0.85	0.72	0.67	0.82	0.7	0.64	0.82	0.74	0.64
3500	0.83	0.7	0.65	0.8	0.68	0.62	0.8	0.72	0.62
4000	0.86	0.73	0.68	0.84	0.72	0.64	0.84	0.76	0.66
4500	0.89	0.76	0.71	0.86	0.74	0.68	0.87	0.79	0.69
5000	0.92	0.79	0.74	0.89	0.77	0.71	0.9	0.82	0.72

International Journal of Recent Development in Engineering and Technology
Website: www.ijrdet.com (ISSN 2347-6435 (Online) Volume 15, Issue 08, August 2026)

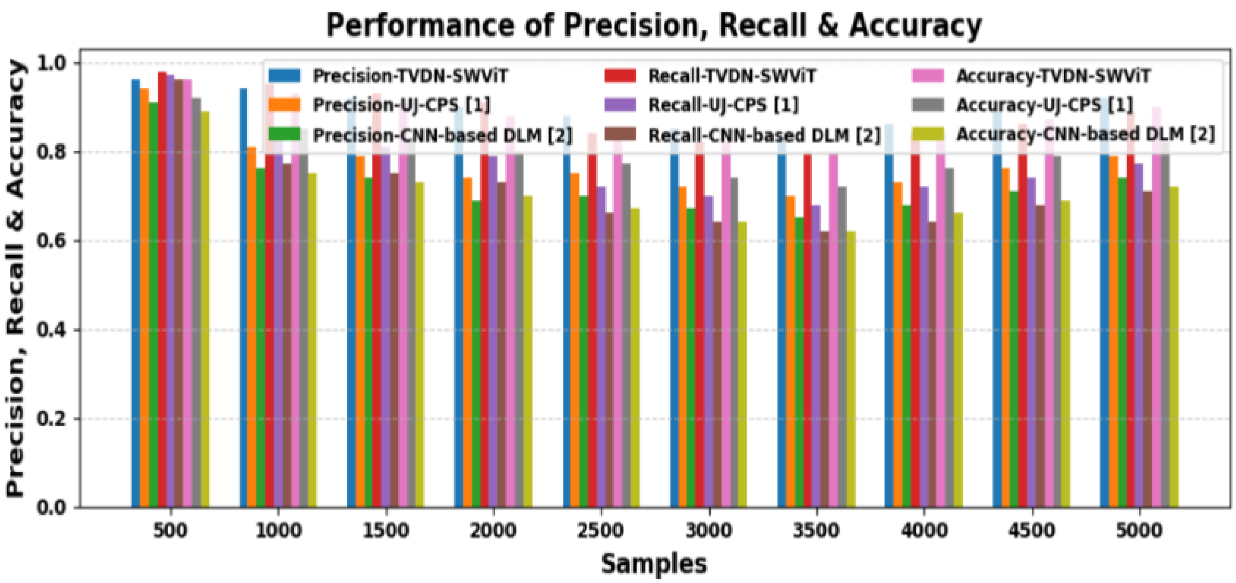

Figure 10 Precision, Recall and Accuracy versus sample slices

Finally figure 10 given above shows the precision, recall and accuracy results of the three methods, TVDN-SWViT, UJ-CPS [1] and CNN-based DLM [2] for samples ranging between 500 and 5000 performed over a simulation of ten runs.

VI. Results And Discussion

The proposed framework should be evaluated through quantitative and qualitative experiments. Since the actual training and testing of the TVDN-SWViT model have not yet been completed, numerical performance values should be inserted only after completing the experiments.
An ablation study should compare DenseNet121, DenseNet with preprocessing, DenseNet with ternary views, DenseNet with partial attention, DenseNet with Transformer, and the complete TVDN-SWViT framework.

VII. Comparison With Existing Approaches

Existing studies provide evidence that deep learning can achieve promising performance in CTA-based aneurysm detection. Earlier research demonstrated automated detection using CTA, while later studies have moved toward large-scale multicenter training and external validation.

A recent integrated deep-learning study investigated aneurysm detection, segmentation, and morphological measurement using CTA and reported strong performance in its study setting.

VIII. Conclusion

Aneurysm detection is a demanding task owing to drawbacks in imaging technology and demanding anatomical locations.Next, a Ternary View Partial Attention DenseNet Feature extraction algorithm is designed to concentrate on local and detailed vascular structures with minimal false positive. Finally Dual Position Shifted Window-based Vision Transformer algorithm using Attribute-based Positional Encoding (APE) and Topology-based Positional Encoding (TPE) along with Shifted Window function in Transformer Encoder results in improved accuracy

REFERENCES

[1] Jianbing Bai, Maolin He, YanliuU, "Uncertainty Guided Joint Cross Pseudo Supervision for Semi-Supervised Intracranial Aneurysm Segmentation", IEEE Access, Vol. 13, Oct 2025 [Uncertainty-guided Joint Cross Pseudo Supervision (UJ-CPS)]

[2] Lu Zeng, Li Wen, Yang Jing, Jing-xu Xu, Chen-cui Huang, Dong Zhang, Guang-xian Wang, "Assessment of the stability of intracranial aneurysms using a deep learning model based on computed tomography angiography", La radiologia medica, Springer Nature Link, Vol. 130, Dec 2024 [Convolutional Neural Network based Deep Learning Model (CNN-based DLM)]

[3] Lina Tao, Yuhan Zhou, Limin Lei, Yajie Wang , Xiaoxu Guo, Yifan Guo , Songwei Yue, "Performance of deep-learning reconstruction combined with metal artifact reduction algorithm for dual-energy computed tomography angiography in intracranial aneurysm coil embolization", Elsevier, Vol. 16, June 2026

[4] Alexandru Barb, Christian Uhl, Louisa Bornhak , Edris El-Sanosy, Matthias Fink, Dittmar Bockler, Johannes Hatzl, Zephyr Study Group Collaborators, "Accuracy of fully automated iliac artery tortuosity measurements in patients with abdominal aortic aneurysm using deep learning", Elsevier, Vol. 195, Feb 2026

[5] Alexandru Lucie Derycke, Asmaa Doudouh, Florian Cotte, Abdelmalek Habi, Jean-Noel Albertini, Antoine Millon, "Validation of a Deep Learning U-Net Algorithm for Multistructure Segmentation of Infrarenal Abdominal Aortic Aneurysms including Lumen, Thrombus, and Calcifications", Elsevier, Vol. 65, Nov 2025

[6] Chunyue Yan, Hang Zhang, Xiaojiao Zhang, Kun Wang, Ming Yang and Fei Wang, "The roles of radiomics and deep learning for automatic detection, stability assessment,and rupture risk prediction in intracranial aneurysms: a systematic review", European Journal of Medical Research, Springer Nature Link, Vol. 31, Dec 2025

[7] Mingxuan Huang, Tiantian Liu, Jiayin Zhang, Xiaoming Su, Hanlin Chen, Miao Li, Jinghan Guo, Kaiyang Zu, Xiaofeng Chen, Yanguo Su, Hengri Cong, Long Yan, Tianyi Yan & Yiming Deng, "Anatomically-guided Masked Autoencoder with Domain-Adaptive Prompting (AMAP) for multimodal cerebral aneurysm detection and segmentation", npj | digital medicine, Dec 2025

[8] Can Yin, Linan H, Shengwu Duan, Xiqing Deng, "Commercial AI platforms improve reproducibility but fail to meet clinical precision thresholds for intracranial aneurysm measurement: implications for serial surveillance", BMC Medical Imaging, Feb 2026

[9] Jiaqi Wang, Juntong Liu, Zhengyuan Xu, Yunfeng Zhou, Mingquan Ye, "M-PointNet: A Multi-Layer Embedded Deep Learning Model for 3D Intracranial Aneurysm Classification and Segmentation", IET Image Processing, Wiley, Jan 2026

[10] Liyong Zhuo, Yu Zhang, Zijun Song, Zhanhao Mo, Lihong Xing, Fengying Zhu, Huan Meng, Lei Chen, Guoxiang Qu, Pengbo Jiang, Qian Wang, Ruonan Cheng, Xiaoming Mi , Lin Liu , Nan Hong , Xiaohuan Cao, Dijia Wu, Jianing Wang PhD, Xiaoping Yin, "Enhancing Radiologists' Performance in Detecting Cerebral Aneurysms Using a Deep Learning Model: A Multicenter Study", Academic Radiology, Elsevier, Vol. 32, Mar 2025